THE JOURNAL OF PHYSICAL CHEMISTRY B
A JOURNAL OF THE AMERICAN CHEMICAL SOCIETY

pubs.acs.org/JPCB

Article

Microsolvation Effects in the Spectral Tuning of Heliorhodopsin

Kithmini Wijesiri and José A. Gascón*

Cite This: J. Phys. Chem. B 2022, 126, 5803−5809

Read Online

ACCESS | Metrics & More | Article Recommendations | Supporting Information

ABSTRACT: Heliorhodopsins (HeR) are a new category of heptahelical transmembrane photoactive proteins with a covalently linked all-*trans* retinal. The protonated Schiff base (PSB) nitrogen in the retinal is stabilized by a negatively charged counterion. It is well-known that stronger or weaker electrostatic interactions with the counterion cause a significant spectral blue- or red-shift, respectively, in both microbial and animal rhodopsins. In HeR, however, while Glu107 acts as the counterion, mutations of this residue are not directly correlated with a spectral shift. A molecular dynamics analysis revealed that a water cluster pocket produces a microsolvation effect on the Schiff base, compensating to various extents the replacement of the native counterion. Using a combination of molecular dynamics and quantum mechanical/molecular mechanics (QM/MM), we study this microsolvation effect on the electronic absorption of the retinylidene Schiff base chromophore of HeR.

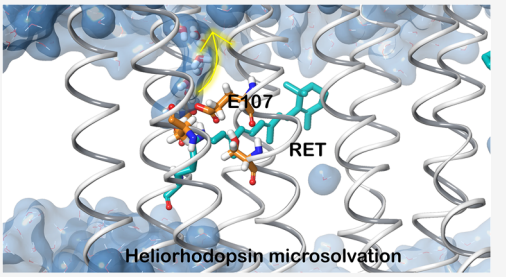

INTRODUCTION

Light-absorbing protein chromophores play critical roles in a variety of biological processes. Their function depends on the modulation of spectroscopic properties through protein−chromophore interactions.[1] Photoreceptors belonging to the rhodopsin family consist of an apoprotein (opsin) and a retinal chromophore covalently bound to the apoprotein by a protonated Schiff base linkage to a special lysine residue. Rhodopsins constitute a large class of membrane proteins that are found in many species, from ancient protobacteria (archaea) to human beings. These proteins convert light into biological signal or chemical energy. Lower organisms utilize a family of microbial rhodopsins for this purpose while the photoreceptor responsible for twilight vision in vertebrate and invertebrate species, belongs to the family of G-protein-coupled receptors. Microbial and animal rhodopsins also termed type-I and type-II rhodopsins, respectively, share no sequence similarity. However, they share similar topologies and contain seven transmembrane α-helices with the N- and C-terminus facing outside and inside of the cell, respectively.[2]

In 2018, using functional metagenomics, Pushkarev et al. discovered a new family of rhodopsins, named heliorhodopsins (HeRs). HeRs are widely present in bacteria, archaea, algae, and algal viruses. They show photocycles that are longer than a second, which is suggestive of light-sensory activity.[3] HeRs are embedded in the membrane with their N-termini facing the cell cytoplasm, an orientation that is opposite to that of type-I or type-II rhodopsins. The interior of HeR's extracellular part is completely hydrophobic. The cytoplasmic part comprises of a Schiff base cavity surrounded by charged amino acids. The cavity contains a cluster of water molecules, presumably being a primary proton acceptor from the Schiff base.[4] In this work, we focus our investigation on HeR-48C12. Two crystallographic structures of HeR-48C12 corresponding to two states of the protein, both solved at 1.50 Å resolution, were obtained in 2020 by Kovalev et al. Authors reported the crystal structure of HeR-48C12 in the violet form at pH 8.8 with a λ_{max} of ∼552 nm (PDB: 6SU3) and the crystal structure of HeR-48C12 in the blue form at pH 4.3 with a λ_{max} of ∼568 nm (PDB: 6SU4).[4] The HeR-48C12 model from the crystal structure, where two protomers are organized as a dimer, is depicted in Figure 1A.

The electrostatic interaction between the positively charged retinal chromophore and the negatively charged counterion has been studied extensively, as it is the dominant component in the regulation of light energy absorption.[5,6] Most microbial rhodopsins contain two counterions at the C-helix and G-helix. Light-driven proton-pump bacteriorhodopsin (BR), has Asp85 in the C-helix and Asp212 in the G-helix as negatively charged counterions. Asp85 and Asp212 are referred to as the primary and secondary counterions, respectively.[7] One of the characteristic features of HeRs is the presence of a single counterion of the Schiff base, similar to the xenorhodopsin family of type-I rhodopsins.[8] In the case of HeR-48C12, Lys241 forms a Schiff base linkage with the all-*trans* retinal chromophore, and its counterion in the C-helix is E107 (Figure 1B). The inactive conformation of the dark state is stabilized by the tight constraints of the cavity and by a salt bridge with the counterion E107. As a consequence of this close interaction, a

Received: May 27, 2022
Revised: July 12, 2022
Published: July 27, 2022

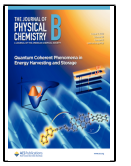

https://doi.org/10.1021/acs.jpcb.2c03672
J. Phys. Chem. B 2022, 126, 5803−5809

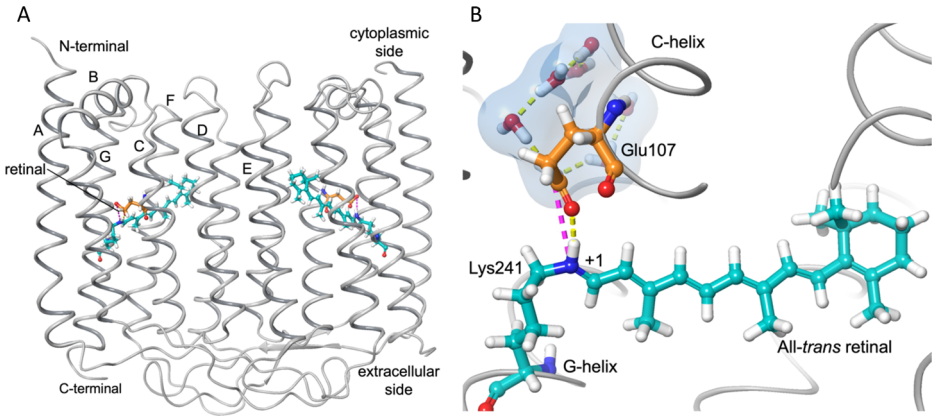

Figure 1. (A) Overall architecture of the dark state of HeR-48C12 dimer (PDB code: 6SU3). The model shows the helix bundle of stabilized rhodopsin with its all-*trans* retinal ligand (teal) forming a Schiff base linkage with the G-helix and a protein counterion (orange) consisting of Glu107 on C-helix. (B) A representative MD snapshot of the Schiff base region. Chromophore retinal (teal) is bound to the protein at Lys241, as well as to the counterion Glu107 (orange). A hydrogen bond and a salt-bridge are observed between the PSB and counterion (yellow and purple dashed lines, respectively). Water molecules in the Schiff base region are represented as ball and stick with a subtle transparent outer surface. The two front helices have been omitted for clarity.

hydrogen bond is formed between the protonated Schiff base (PSB) and E107.

It is well-known that stronger or weaker electrostatic interactions with the counterion cause a spectral blue- or red-shift, respectively, in both type-I and type-II rhodopsins.[9] However, a recent mutagenesis study, which examined possible anion binding into the wild-type and E107 mutants of HeR-48C12, reported identical absorbances for the wild-type and E107D and E107A mutants.[7] This result is unexpected because the length of the side chain is different between Glu and Asp, and because the methyl group of Ala has no hydrogen-bonding potential and no permanent dipole. Moreover, a substantial red-shifted absorbance was observed for the case of E107Q. In the E-to-D mutation, in particular, although the functional acid group is conserved, the shorter side chain leads to an altered local geometry and thus to a different interaction of retinal and protein. As a result, E107D mutation should display a larger, red-shifted absorption than the wild type, by weakening of the direct interaction (i.e., salt bridge) between the PSB and the counterion. This is in fact what has been observed for other rhodopsin proteins.[9−11] However, for HeR this effect is not observed. Motivated by this question, we combined Molecular Dynamics simulations with electronic structure calculations to characterize the effect of E-to-D, E-to-A, and E-to-Q mutations in HeR-48C12. Spectroscopic and kinetic measurements from previous studies have demonstrated that water strongly influences retinal-protein interaction. Water molecules inside proteins often play an important role in proteins' functions. For instance, the long-range proton transfer inside of proteins is usually carried out by the Grotthuss mechanism[12] and requires a chain of hydrogen bonds that is composed of internal water molecules and amino acid residues of the protein. Water also has the potential of screening electrostatic interactions, which can lead to stabilization of charge on ionizable residues.[13] In this work, we observe the presence of a cluster of water molecules in close vicinity to the SB group of the chromophore. Not only this water cluster seems to be essential for the function of HeRs chromophore by stabilizing the chromophore's cavity,[14] but it also appears, as we will show, to reorganize polar residues around the counterion to buffer the absorption spectrum due to microsolvation changes around the Schiff's base. We provide an understanding of the origin of the spectral features observed in experimental studies for various mutants by means of a combination of molecular dynamic (MD) simulations and quantum mechanical/molecular mechanical (QM/MM) calculations.

COMPUTATIONAL METHODS

System Preparation. We started from the highest resolution X-ray structure available for HeR-48C12 (PDB: 6SU3, resolution 1.50 Å) in the violet form solved at pH 8.8. Since dimerization is required for the function of HeRs,[15] the crystal structure of the two protomers was used. The protein and the retinal were processed with Maestro (Schrödinger Release 2021-2). E107 serves as the retinylidene Schiff base counterion in HeR-48C12. The structures for the mutant HeRs were generated by replacing the side chain atoms of the E107 amino acid in the wild-type protein by the residues Asp (E107D), Ala (E107A), and Gln (E107Q). The X-ray structures are derived from measurements performed in crystallized proteins at cryogenic temperatures, and the water positions observed in such structural models may differ from those at room temperature under physiological conditions. The atomic details of water distribution depend on the dynamics of the water molecules and can be probed via Molecular Dynamics simulations. Water molecules near the Schiff base could play an important role in the formation of an extended hydrogen bonded network for proton transfer.[16,17] Consequently, the crystallographic waters near the Schiff base were kept. All other molecules in the X-ray structure OLC, LFA, OLA, SO_4^{-2}, and GOL were deleted. The protein preparation application within Maestro was used in preprocessing the complex, assigning bond orders, adding hydrogens, and filling in missing loops. For the alternative positions of side chains reported in the crystal structures, the most populated ones were kept (i.e., according to the pdb β-factor). Optimization of hydrogen-bond assignment was performed at pH 8.8, which was the pH used for previous mutation studies of HeR-48C12[7,9] and later at pH 4.3 for the acidic structure. A restrained minimization was applied for hydrogens only. The protein dimer was embedded in a predefined POPC (1-palmitoyl-2-oleoyl-*sn*-glycero-3-phosphatidylcholine) mem-

https://doi.org/10.1021/acs.jpcb.2c03672
J. Phys. Chem. B 2022, 126, 5803−5809

brane. A 10 Å buffer size, orthorhombic box was constructed using the TIP3P water model.[18] The PROPKA method,[19] within the protein preparation software, was used to determine the protonation states and tautomerization of all amino acids depending on the pH. Despite the differences in pH, PROPKA assigned the same protonation states and tautomerization for both pH states, resulting in a total charge of +5e for both pHs. Note, however, that in the last section of this work we do investigate various protonation states for the pair PSB-Glu107. Cl^- ions were added to neutralize the positive charge of the system. Additionally, a salt concentration of 0.15 M NaCl was added to the system. The entire system contained approximately 58 000 atoms. All preliminary minimizations and MD simulations used the force field OPLS4.[20] OPLS4, which is based on the original OPLS force field, incorporates an extended torsional parametrization as well as optimized partial charge assignment.

Molecular Dynamics Simulations. MD simulations were carried out on Nvidia GPU hardware with Desmond (Schrödinger Release 2021-2). Pre-equilibration of the system was carried out via the following procedure: first, an equilibration was performed for 50 ps using Brownian dynamics under the *NVT* ensemble at a temperature of 10 K applying restraints on the solute with a force constant 50 kcal mol^{-1} $Å^{-2}$. Next, a 20 ps classical MD simulation (CMD) at a temperature of 100 K and a pressure 1000 bar, restraining the solute and membrane heavy atoms with a force constant of 50 kcal mol^{-1} $Å^{-2}$, followed by a relaxation under the NP_AT (constant normal pressure, lateral surface area of membrane, and constant temperature) ensemble at the same temperatures and pressures for 100 ps. Restraints were placed on the solute heavy atoms (force constant 10 kcal mol^{-1} $Å^{-2}$) and on the membrane N and P atoms in the *z*-direction (force constant 2 kcal mol^{-1} $Å^{-2}$). Under the same restraints, the gradual heating of the system was conducted via 150 ps CMD simulations under the NP_AT ensemble from 100 to 300 K, at a pressure of 100 bar. The restraints were gradually reduced to 0 at this stage. Finally, a 50 ps classical MD simulation under the *NVT* ensemble at a temperature of 300 K was performed by applying restraints on the protein backbone and the ligand heavy atoms with a force constant 5 kcal mol^{-1} $Å^{-2}$. The pre-equilibrated structures were used as the initial structures for the subsequent MD simulations. Note that the restraints were completely eliminated after the pre-equilibration with the CMD simulations. Temperature and pressure were kept with the Nosé–Hoover thermostat and the Martyna–Tobias–Klein barostat, respectively. Classical MD simulations were run for a total time of 200 ns using the NP_AT ensemble (300 K, 1 atm) for each system. We extracted 50 configurations that were saved during the last 100 ns of the MD simulation at a 2 ns interval. These structures were then used for the calculation of excitation energies at the QM/MM level.

Correlation Time. We estimated the correlation time in our MD simulation by considering the distance between the NH of the PSB and the C in the COO− group of Glu117 in the wild type system, which is a critical distance that tunes the absorption spectrum. This distance was used to calculate block averages and the block standard error (BSE). Following the work of Grossfield et al.,[21] the correlation time was estimated by first computing the minimum block length after which the BSE reaches a plateau. With the estimation of the BSE, we then computed a correlation time of ∼0.5 ns. Thus, the 2 ns sampling interval is well justified.

Additional information about the MD analysis, including protein–ligand RMSD (root-mean-square deviation) calculation, RMSDs of critical residues, and description of protein–ligand interactions monitored throughout the simulation, is reported in the Supporting Information (Figures S1–S4 and Table S1).

Structure Optimizations and Electronic Structure Calculations. The QM/MM boundary was placed between the C_γ and C_β of Lys241 using the hydrogen link method. The QM part, consisting of the retinal molecule and part of Lys241's side chain, was described using the B3LYP functional. The rest of the protein, POPC membrane and the solvents were treated at the MM level using the OPLS4 force field, while the water molecules were described using the TIP3P model. Previous studies have applied especially developed force fields to describe retinal dynamics of microbial and animal rhodopsins, allowing for a direct calculation of QM-derived electronic properties from MD snapshots.[22,23] We chose a different approach, which we recently implemented in the study of spectral properties of carotenoid proteins,[24,25] where the MD snapshots are partially optimized at the QM/MM level. This is done to refine the bond length alternation (BLA) of the chromophore, which is largely overestimated by the force field. These local optimizations were performed at the DFT B3LYP/6-31G* level only relaxing the QM region (i.e., the rest protein, POPC bilayer and solvent remain frozen). Considering only the QM region, the in-place RMSD before and after QM/MM minimization is, on average, 0.02 Å. Thus, while the local QM/MM minimizations produce very small displacements within the protein cavity it produces high quality structures in the QM/MM configurational space. The B3LYP/6-31G* level of theory has proven very reliable to obtain accurate geometries in retinal molecules[26] and other isoprenoid-based molecules such as carotenoids.[25] Excited state energies were then calculated from the optimized structures by means of the DFT SVWN/6-31G*. SVWN was chosen as it is the functional that best reproduces the excitation energy of the isolated all-*trans* *n*-butyl retinal in gas phase.[27] Other functionals we consider include B3LYP, BPW91, and BP86 (*vide infra*).

RESULTS AND DISCUSSION

Basic Principles of Opsin Shift. In the ground state, the retinal chromophore is positively charged and becomes stabilized by the counterion Glu107. The excited state has a charge transfer character presenting a slight migration of the positive charge toward the β-ionone ring. Thus, the presence of the counterion stabilizes the ground state more than it stabilizes the excited state. This results in a larger energy gap between ground and excited states compared to the case of the retinal chromophore in the gas phase or when surrounded by a nonpolar environment. This causes a blue shift in the absorption spectrum (opsin shift). As the single negative charge is moved away from the PSB or is removed all together, the energy gap becomes smaller and the shift reverses to the red. Thus, in principle, the E-to-D, E-to-A, and E-to-Q mutations should all exert a red-shift, as it occurs in other type I and type II rhodopsin species.[25,28,29] As we will show below, however, these basic principles are altered by microsolvation effects in heliorhodopsin.

QM/MM on the MD Trajectory. The MD for wild type HeR shows a stable RMSD for the protein (∼1.98 Å ± 0.1 Å) and the ligand (∼0.73 Å ± 0.1 Å) for the production interval

https://doi.org/10.1021/acs.jpcb.2c03672
J. Phys. Chem. B 2022, 126, 5803−5809

(100 ns −200 ns), and similar RMSD values are found for the mutant cases (Figures S1−S4). The vertical excitation energies (λ_{max} in nm) and oscillator strengths (f) of the all-*trans* retinal were calculated by B3LYP, BPW91, BP86, and SVWN with the 6-31G* basis set and the calculated results were compared with the experimental values in Table 1.[30] Results show that

Table 1. Single Point QM Calculations of λ_{max} and Oscillatory Strengths (f) on Optimized Structures at the B3LYP/6-31G* Level Taken from MD Simulations of Wild-Type and Mutants[a]

model	level of theory (6-31G*)	λ_{max}/nm	f	exptl λ_{max}/nm
wild	SVWN	533.3	1.3	552
	BPW91	529.3	1.3	
	BP86	529.1	1.3	
	B3LYP	478.5	1.9	
E107D	SVWN	536.5	1.3	552
	BPW91	532.2	1.3	
	BP86	532.0	1.3	
	B3LYP	483.4	1.9	
E107A	SVWN	535.8	1.4	552
	BPW91	531.5	1.4	
	BP86	531.3	1.3	
	B3LYP	486.1	2.0	
E107Q	SVWN	543.2	1.3	575
	BPW91	538.6	1.3	
	BP86	538.4	1.3	
	B3LYP	490.5	1.9	

[a]Results are expressed as the mean of 50 snapshots. Standard deviation of λ_{max}, f and 95% confidence intervals are presented in the Supporting Information (Table S2). Typical confidence intervals are ∼4−5 nm.

different functionals do affect the calculated absorbances and oscillatory strengths. The closest calculated λ_{max} = 536 nm (experimental value 552 nm) is predicted by SVWN/6-31G*, which is consistent with the benchmark produced by Sun et al. in a time-dependent density functional theory investigation of gas-phase Schiff base retinal chromophores.[27] Besides this quantitative agreement with SVWN, it is worth noting that all level of theories reproduce the shifts, or lack thereof, from wild type to mutant, within the calculated intervals of confidence (Table S2).

It is interesting to note that the microsolvation cluster that emerges from our MD simulations of the wild-type protein is very stable throughout the simulations in both monomers (Figure 3). We counted the number of waters molecules residing in the cavity within a radius of 10 Å from the Schiff base nitrogen and obtained an average number between 7 and 9, depending on the mutant. We also observed that such a number is roughly constant during the simulation. Visual inspection of trajectory snapshots, however, clearly shows that the identity of these water molecules is not maintained. Thus, we infer that there is exchange of waters between the cavity and the cytoplasm. Taking into account the absence of charged amino acids in the hydrophobic extracellular internal part of the protein and that proton is not transiently released to the aqueous phase, this is in line with the analysis by Kovalev et al. that argued that such water cluster is a candidate for the proton acceptor.[4] They further suggested that this cavity mediates proton storage in the aqueous phase after its release from the PSB, which then returns to the PSB at the end of the photocycle.

Analysis of the Retinal Binding Pocket and PSB Region for Wild-Type and Mutants. To evaluate the effect of the mutations on spectral shifts, we compared the retinal binding pocket and counterion interactions in the wild-type and the mutated structures. In the wild-type structure, the side chain oxygen atoms of the counterion are close to the retinal Schiff base nitrogen (OE1 and OE2 are, on average, 2.9 and 4.1 Å from the PSB nitrogen, respectively). The carboxylate oxygen OE2 is typically oriented away from the conjugated retinal chain (as shown by the representative snapshot in Figure 2). A polar interaction network around the PSB−counterion complex is observed in this configuration. The PSB is hydrogen-bonded directly to Glu107, consistent with a previous resonance Raman analysis.[31] A salt bridge is present between the atoms forming the PSB linkage and the counterion. A hydrogen bond is also maintained between PSB and Ser237. The counterion's carboxylate forms hydrogen

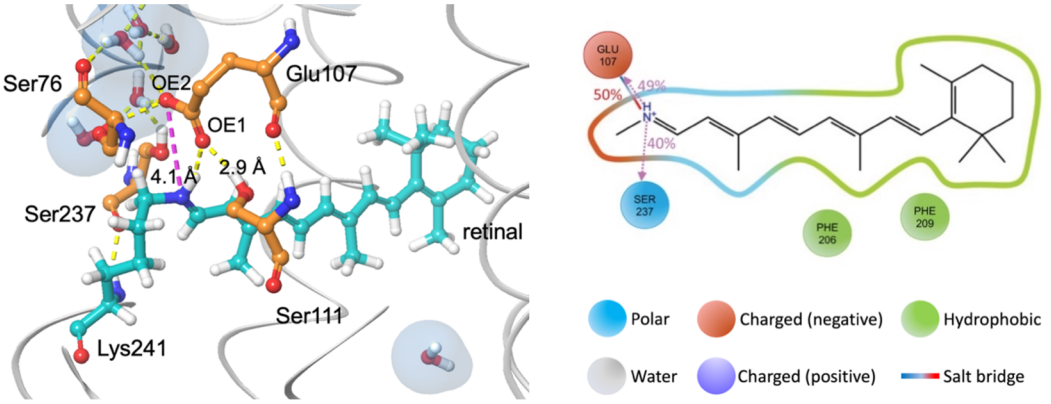

Figure 2. (Left) Representative MD snapshot followed by a QM/MM optimization at around 150 ns for wild type HeR-48C12. Hydrogen bonds and salt-bridges are indicated by yellow and purple dashed lines, respectively. Water molecules are represented with a subtle transparent molecular surface. (Right) Average occurrence contacts in the form of a 2-D interaction diagram. Different interaction types are indicated by color and line type. Interactions that occur more than 30.0% of the simulation time in the selected trajectory are shown. Criteria that define specific interactions (i.e., hydrogen-bonds and salt bridges) are detailed in the Supporting Information. Violet dashed line arrows indicate hydrogen bonds. Arrows are drawn from the H-bond donor to the H-bond acceptor. Solid and dashed violet lines indicate backbone and side chain hydrogen bonds, respectively.

https://doi.org/10.1021/acs.jpcb.2c03672
J. Phys. Chem. B 2022, 126, 5803−5809

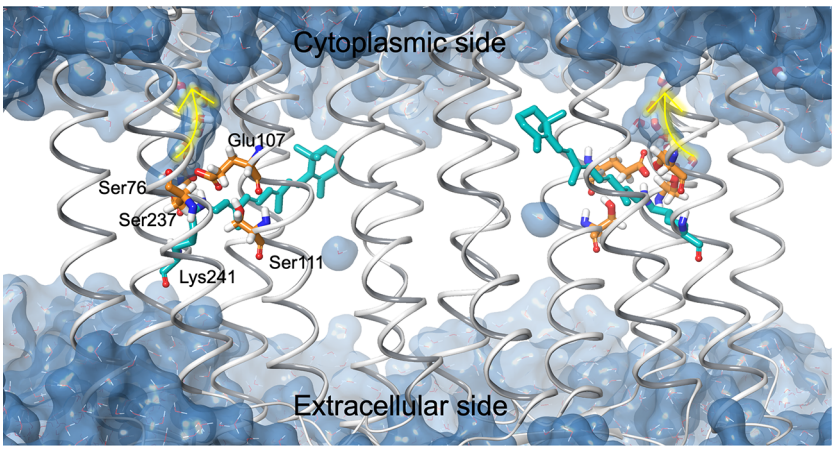

Figure 3. Stable microsolvation cluster in the Schiff base cavity that can act as the primary proton acceptor from the Schiff base. Arrows indicate the path toward the cytoplasm.

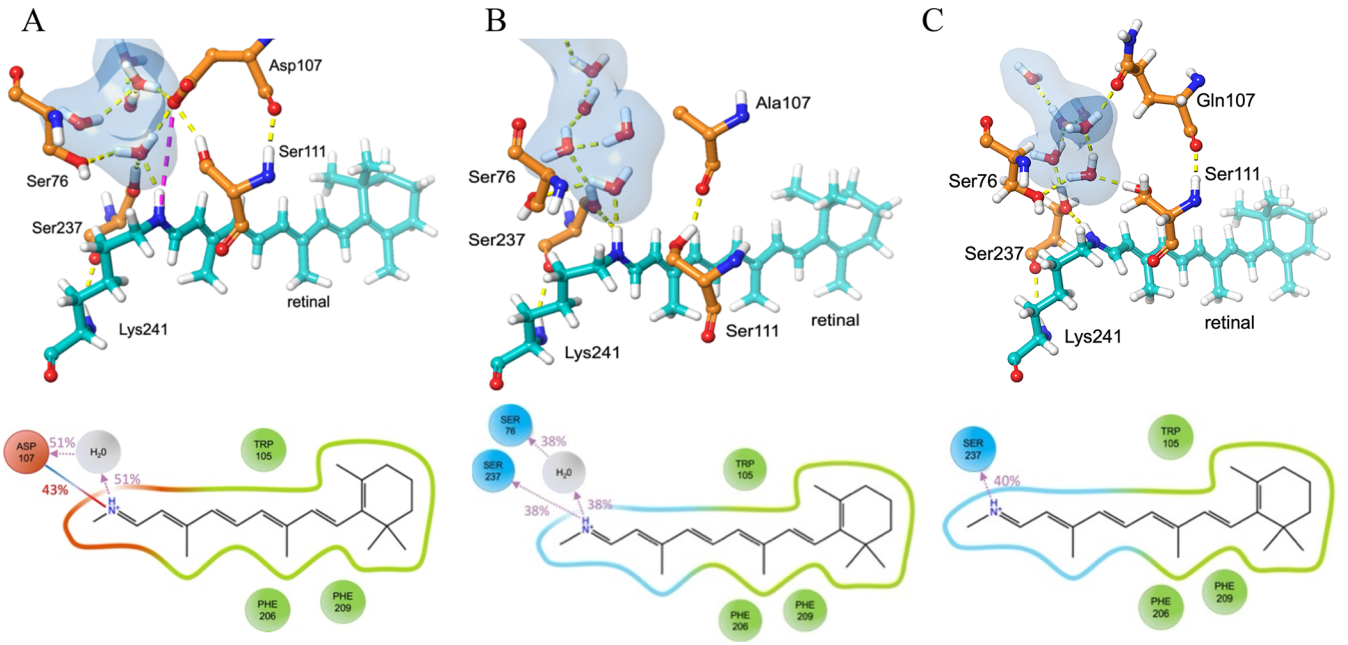

Figure 4. Representative snapshots from an optimized QM/MM model indicating the interactions of the PSB and water molecules for the mutated models and their respective interactions diagrams. Note that on the top panel H-bonds are indicated by yellow lines, while in the bottom panel they are indicated with dashed arrowed lines. (A) E107D at 171 ns, (B) E107A at 162 ns, and (C) E107Q at 142 ns along with the surrounding polar amino acid residues are represented as balls and sticks. These snapshots are chosen to be representative of the average occurrences obtained in the simulation interaction diagram (bottom panel).

bonds with Ser76, Ser111 and the NH+ of the PSB. Note that the simulations do not show a water between the counterion and PSB. The interaction between the counterion and the PSB is too compact in the wild-type to permit microsolvation of the PSB. Thus, the sole stabilization of the positively charged in the PSB arises through direct hydrogen bond interactions (49% occurrence to Glu107 and 40% to Ser237) and the salt bridge with the Glu107 (50%).

The E107D mutation rearranges the polar interaction network around the PSB−counterion complex. While this mutation conserves the counterion character, the distances from the PSB nitrogen to OD1 and OD2 are now ∼5.2 and ∼4.9 Å on average, respectively. This distance is too far for the Schiff base to form a direct hydrogen bond (Figure 4A). However, the charged carboxylate of Asp107 maintains the salt-bridge between the positive charge on the Schiff base nitrogen as well as the hydrogen bonding interactions with Ser76 and Ser111. What becomes crucially different now is that simulations show a microsolvation around the PSB with a consistent hydrogen bond to a single water molecule with a 51% occurrence (Figure 4A).

Substitution of alanine at the Glu107 position removes the counterion. The distance from the PSB nitrogen to alanine's CH_3 group is ∼8 Å, which creates a considerably large cavity around the Schiff base. Consequently, the PSB forms a consistent hydrogen bond directly to Ser237, and a water cluster microsolvates the PSB as in the case of E107D.

In E107Q, the side chain volume is not drastically altered. Consequently, the PSB forms a consistent hydrogen bond with Ser237, as it occurs in the wild type. While water molecules still reside inside the cavity in E107Q, as in the other mutants, hydrogen bonds with water molecules are considerably

https://doi.org/10.1021/acs.jpcb.2c03672
J. Phys. Chem. B 2022, 126, 5803−5809

reduced, creating a less polar environment. All the specific protein−ligand interactions monitored throughout the simulation are described in the Supporting Information (Figures S5−S8).

Given the observed differences in the interactions and microsolvation around the Schiff base, we can now explain the unexpected behavior in the absorption spectrum observed experimentally and reproduced by our calculated finite temperature averages. Recall that (1) the calculated λ_{max} values for the wild-type, E107D and E107A are roughly identical within the calculated interval of confidence (consistent with the experiments), even though the distance between the PSB and the counterion's carboxylate in E107D is substantially larger and in E107A the counterion is removed altogether; (2) calculations in E107Q show a statistically significant red-shift of ∼10 nm, consistent with the experiments (see the Supporting Information for all ANOVA analyses of maximum absorbance shifts). To understand why E107D and E107A mutations do not cause a spectral shift, we closely examined the PSB region of each mutant and compared it with that of the wild type. As shown in Figure 4, we observed water molecules entering the cavity between the Schiff base and the counterion forming strong, stable hydrogen bonds with the PSB. Thus, the absence of a close counterion in these two mutants rearranges the cavity and produces a close-knit polar environment around the PSB. Therefore, this produces the same opsin shift as in the case of the wild type.

In the E107Q model, water molecules do not form hydrogen bonds with PSB (Figure 4C). Instead, several water molecules are seen to form hydrogen bonds with the side chain of Q107. The only stabilizing effect we see in E107Q is a hydrogen bond formed between the Schiff base nitrogen and the Ser237.

Structure of HeR-48C12 at Acidic pH: Purple-to-Blue Transition. To investigate the conformational rearrangements in the HeR associated with decrease in pH, we performed a 200 ns MD simulation starting with the HeR-48C12 crystal structure, which was derived at pH 4.3 (PDB code: 6SU4). In principle, the pH of the surrounding solution can cause conformational rearrangements to the structure of HeR due to protonation or deprotonation of key residues. However, according to the two crystal structures, the backbone organization and the location of most of the residues at pH 4.3 remains practically the same as in the high 8.8 pH structure (RMSD = 0.158 Å).[4] Interestingly, at acidic pH, a planar triangular molecule (acetate) is present in the Schiff base cavity. However, this acetate is not observed in the neutral pH crystal structure. While the crystal packing is the same as in the crystals grown at high pH, decreasing the pH from 8.8 to 4.3 causes a ∼16 nm red shift in the absorption maximum from 552 to 568 nm in a dark-adapted WT. It was suggested that this so-called purple-to-blue transition is caused by protonation of Glu107.[32] To test this hypothesis, we performed MD simulations of 6SU4 with Glu107 protonated. MD simulations followed by hybrid QM/MM calculations were performed for two models: acetate anion and protonated acetate to evaluate its effect on the HeR-48C12 absorption spectrum. With the SVWN/6-31G* level of theory, a slight shift of the absorbance (∼2 nm) can be observed for protonated Glu107 model in the presence of acetate anion. Interestingly, when the acetate is protonated due to the low pH, a statistically significant red shift of ∼6 nm was obtained. Absorption with other functionals, standard deviation of λ_{max} and f are presented in the Supporting Information (Table S3), as well as an ANOVA analysis. Comparing the pH 4.3 and pH 8.8 structures, the distance between the Glu107 oxygen and the Schiff base nitrogen is 3.3 Å at pH 4.3 and 2.9 Å at pH 8.8. At acidic pH, Glu107 does not interact with the PSB (Figure S9), but at high pH it creates a strong hydrogen bond with the PSB (Figure 2). Thus, the 6 nm red shift can be explained within the same framework as the shifts discussed in the mutation analysis (*vide supra*). That is, the loss of interaction with Glu107, and the absence of microsolvation around the PSB (Figure S9) makes the NH+ of PSB to solely interact with Ser237, similar to the mutation E107Q in the high pH simulation (Figure 4C).

CONCLUSIONS

In this work, we examined the absorption spectrum of wild-type Heliorhodopsin and several mutants using a multilayered MD/QM/MM approach. A key technical aspect is the targeted minimization at the QM/MM level to correct for inaccuracies in the force field sampling of the retinal's configurational space. A detailed correlation between absorbance a simulation interaction diagrams offers a powerful approach for the analysis of spectral tuning in photoactive proteins.

We observed similar absorbances for wild-type, E107D, and E107A, whereas E107Q showed a significant red shift, in agreement with the experimental data. In wild type, the protonated retinal Schiff base is stabilized by its counterion E107. In E107D and E107A, the weaker interaction with the PSB allows microsolvation of the PSB with a consistent hydrogen bond between PSB and a water molecule, substantially stabilizing the ground state. This stabilization compensates for the weakening/removal of the PSB−counterion salt bridge and produces no net opsin-shift, contrary to what has been observed for other rhodopsin proteins. The E107Q mutation is a special case. Glutamine is a neutral amino acid residue which cannot stabilize the PSB. However, contrary to what occurs for the other mutants, the E107Q mutation does not considerably alter the side chain volume and does not permit a hydrogen bond between the PSB and nearby water molecules. This produces the red-shift known to occur in rhodopsin proteins as a result of counterion removal.

ASSOCIATED CONTENT

Supporting Information

The Supporting Information is available free of charge at https://pubs.acs.org/doi/10.1021/acs.jpcb.2c03672.

MD methods, MD analysis (RMSD (root mean square deviation) plots, RMDs of key residues, and protein−ligand interactions), QM calculations on optimized models from MD for 6SU3 wildtype and mutated models, QM calculations on optimized models from MD for 6SU4 wildtype, box plots and normality test, and one-way analysis of variance (ANOVA) test (PDF)

AUTHOR INFORMATION

Corresponding Author

José A. Gascón − *Department of Chemistry, University of Connecticut, Storrs, Connecticut 06269-3060, United States;* orcid.org/0000-0002-4176-9030; Email: jose.gascon@uconn.edu

Author

Kithmini Wijesiri − *Department of Chemistry, University of Connecticut, Storrs, Connecticut 06269-3060, United States*

https://doi.org/10.1021/acs.jpcb.2c03672
J. Phys. Chem. B 2022, 126, 5803−5809

Complete contact information is available at:
https://pubs.acs.org/10.1021/acs.jpcb.2c03672

Notes

The authors declare no competing financial interest.

■ ACKNOWLEDGMENTS

This work was supported by the National Science Foundation, Award CHE-1904700 (to J.A.G). Computational resources for this work have been provided through the University of Connecticut Storrs HPC center.

■ REFERENCES

(1) Wang, W.; Nossoni, Z.; Berbasova, T.; Watson, C. T.; Yapici, I.; Lee, K. S. S.; Vasileiou, C.; Geiger, J. H.; Borhan, B. Tuning the Electronic Absorption of Protein-Embedded All- *Trans* -Retinal. *Science* **2012**, *338* (6112), 1340−1343.
(2) Ernst, O. P.; Lodowski, D. T.; Elstner, M.; Hegemann, P.; Brown, L. S.; Kandori, H. Microbial and Animal Rhodopsins: Structures, Functions, and Molecular Mechanisms. *Chem. Rev.* **2014**, *114* (1), 126−163.
(3) Pushkarev, A.; Inoue, K.; Larom, S.; Flores-Uribe, J.; Singh, M.; Konno, M.; Tomida, S.; Ito, S.; Nakamura, R.; Tsunoda, S. P.; Philosof, A.; Sharon, I.; Yutin, N.; Koonin, E. V.; Kandori, H.; Béjà, O. A Distinct Abundant Group of Microbial Rhodopsins Discovered Using Functional Metagenomics. *Nature* **2018**, *558* (7711), 595−599.
(4) Kovalev, K.; Volkov, D.; Astashkin, R.; Alekseev, A.; Gushchin, I.; Haro-Moreno, J. M.; Chizhov, I.; Siletsky, S.; Mamedov, M.; Rogachev, A.; Balandin, T.; Borshchevskiy, V.; Popov, A.; Bourenkov, G.; Bamberg, E.; Rodriguez-Valera, F.; Büldt, G.; Gordeliy, V. High-Resolution Structural Insights into the Heliorhodopsin Family. *Proc. Natl. Acad. Sci. U. S. A.* **2020**, *117* (8), 4131−4141.
(5) Gascón, J. A.; Sproviero, E. M.; Batista, V. S. QM/MM Study of the NMR Spectroscopy of the Retinyl Chromophore in Visual Rhodopsin. *J. Chem. Theory Comput.* **2005**, *1* (4), 674−685.
(6) Vreven, T.; Morokuma, K. Investigation of the S0 to S1 Excitation in Bacteriorhodopsin with the ONIOM(MO:MM) Hybrid Method. *Theor. Chem. Acc.* **2003**, *109* (3), 125−132.
(7) Singh, M.; Katayama, K.; Béjà, O.; Kandori, H. Anion Binding to Mutants of the Schiff Base Counterion in Heliorhodopsin 48C12. *Phys. Chem. Chem. Phys.* **2019**, *21* (42), 23663−23671.
(8) Higuchi, A.; Shihoya, W.; Konno, M.; Ikuta, T.; Kandori, H.; Inoue, K.; Nureki, O. Crystal Structure of Schizorhodopsin Reveals Mechanism of Inward Proton Pumping. *Proc. Natl. Acad. Sci. U.S.A.* **2021**, *118* (14), No. e2016328118.
(9) Tanaka, T.; Singh, M.; Shihoya, W.; Yamashita, K.; Kandori, H.; Nureki, O. Structural Basis for Unique Color Tuning Mechanism in Heliorhodopsin. *Biochem. Biophys. Res. Commun.* **2020**, *533* (3), 262−267.
(10) Nagata, T.; Koyanagi, M.; Tsukamoto, H.; Mutt, E.; Schertler, G. F. X.; Deupi, X.; Terakita, A. The Counterion-Retinylidene Schiff Base Interaction of an Invertebrate Rhodopsin Rearranges upon Light Activation. *Commun. Biol.* **2019**, *2* (1), 180.
(11) Scholz, F.; Bamberg, E.; Bamann, C.; Wachtveitl, J. Tuning the Primary Reaction of Channelrhodopsin-2 by Imidazole, PH, and Site-Specific Mutations. *Biophys. J.* **2012**, *102* (11), 2649−2657.
(12) Agmon, N. The Grotthuss Mechanism. *Chem. Phys. Lett.* **1995**, *244* (5−6), 456−462.
(13) Morozenko, A.; Leontyev, I. V.; Stuchebrukhov, A. A. Dipole Moment and Binding Energy of Water in Proteins from Crystallographic Analysis. *J. Chem. Theory Comput.* **2014**, *10* (10), 4618−4623.
(14) Schobert, B.; Brown, L. S.; Lanyi, J. K. Crystallographic Structures of the M and N Intermediates of Bacteriorhodopsin: Assembly of a Hydrogen-Bonded Chain of Water Molecules Between Asp-96 and the Retinal Schiff Base. *J. Mol. Biol.* **2003**, *330* (3), 553−570.
(15) Lu, Y.; Zhou, X. E.; Gao, X.; Wang, N.; Xia, R.; Xu, Z.; Leng, Y.; Shi, Y.; Wang, G.; Melcher, K.; Xu, H. E.; He, Y. Crystal Structure of Heliorhodopsin 48C12. *Cell Res.* **2020**, *30* (1), 88−90.
(16) Papadopoulos, G.; Dencher, N. A.; Zaccai, G.; Büldt, G. Water Molecules and Exchangeable Hydrogen Ions at the Active Centre of Bacteriorhodopsin Localized by Neutron Diffraction. *J. Mol. Biol.* **1990**, *214* (1), 15−19.
(17) Gerwert, K.; Freier, E.; Wolf, S. The Role of Protein-Bound Water Molecules in Microbial Rhodopsins. *Biochim. Biophys. Acta Bioenerg.* **2014**, *1837* (5), 606−613.
(18) Jorgensen, W. L.; Chandrasekhar, J.; Madura, J. D.; Impey, R. W.; Klein, M. L. Comparison of Simple Potential Functions for Simulating Liquid Water. *J. Chem. Phys.* **1983**, *79* (2), 926−935.
(19) Bas, D. C.; Rogers, D. M.; Jensen, J. H. Very Fast Prediction and Rationalization of PKa Values for Protein-Ligand Complexes. *Proteins* **2008**, *73* (3), 765−783.
(20) Lu, C.; Wu, C.; Ghoreishi, D.; Chen, W.; Wang, L.; Damm, W.; Ross, G. A.; Dahlgren, M. K.; Russell, E.; Von Bargen, C. D.; Abel, R.; Friesner, R. A.; Harder, E. D. OPLS4: Improving Force Field Accuracy on Challenging Regimes of Chemical Space. *J. Chem. Theory Comput.* **2021**, *17* (7), 4291−4300.
(21) Grossfield, A.; Patrone, P. N.; Roe, D. R.; Schultz, A. J.; Siderius, D.; Zuckerman, D. M. Best Practices for Quantification of Uncertainty and Sampling Quality in Molecular Simulations. *Living J. Comp. Mol. Sci.* **2019**, *1* (1), 5067.
(22) Doemer, M.; Maurer, P.; Campomanes, P.; Tavernelli, I.; Rothlisberger, U. Generalized QM/MM Force Matching Approach Applied to the 11-Cis Protonated Schiff Base Chromophore of Rhodopsin. *J. Chem. Theory Comput.* **2014**, *10* (1), 412−422.
(23) Ryazantsev, M. N.; Nikolaev, D. M.; Struts, A. V.; Brown, M. F. Quantum Mechanical and Molecular Mechanics Modeling of Membrane-Embedded Rhodopsins. *J. Membr. Biol.* **2019**, *252* (4−5), 425−449.
(24) Clark, K.; Pigni, N. B.; Wijesiri, K.; Gascón, J. A. Spectral Features of Canthaxanthin in HCP2. A QM/MM Approach. *Molecules* **2021**, *26* (9), 2441.
(25) Pigni, N. B.; Clark, K. L.; Beck, W. F.; Gascón, J. A. Spectral Signatures of Canthaxanthin Translocation in the Orange Carotenoid Protein. *J. Phys. Chem. B* **2020**, *124* (50), 11387−11395.
(26) Gascón, J. A.; Sproviero, E. M.; Batista, V. S. Computational Studies of the Primary Phototransduction Event in Visual Rhodopsin. *Acc. Chem. Res.* **2006**, *39* (3), 184−193.
(27) Sun, M.; Ding, Y.; Cui, G.; Liu, Y. S_1 and S_2 Excited States of Gas-Phase Schiff-Base Retinal Chromophores: A Time-Dependent Density Functional Theoretical Investigation. *J. Phys. Chem. A* **2007**, *111* (15), 2946−2950.
(28) Sulkes, M.; Lewis, A.; Lemley, A. T.; Cookingham, R. Modeling the Resonance Raman Spectrum of a Metarhodopsin: Implications for the Color of Visual Pigments. *Proc. Natl. Acad. Sci. U.S.A.* **1976**, *73* (12), 4266−4270.
(29) Honig, B.; Ebrey, T.; Callender, R. H.; Dinur, U.; Ottolenghi, M. Photoisomerization, Energy Storage, and Charge Separation: A Model for Light Energy Transduction in Visual Pigments and Bacteriorhodopsin. *Proc. Natl. Acad. Sci. U. S. A.* **1979**, *76* (6), 2503−2507.
(30) Singh, M.; Inoue, K.; Pushkarev, A.; Béjà, O.; Kandori, H. Mutation Study of Heliorhodopsin 48C12. *Biochemistry* **2018**, *57* (33), 5041−5049.
(31) Otomo, A.; Mizuno, M.; Singh, M.; Shihoya, W.; Inoue, K.; Nureki, O.; Béjà, O.; Kandori, H.; Mizutani, Y. Resonance Raman Investigation of the Chromophore Structure of Heliorhodopsins. *J. Phys. Chem. Lett.* **2018**, *9* (22), 6431−6436.
(32) Imasheva, E. S.; Balashov, S. P.; Ebrey, T. G.; Chen, N.; Crouch, R. K.; Menick, D. R. Two Groups Control Light-Induced Schiff Base Deprotonation and the Proton Affinity of Asp85 in the Arg82His Mutant of Bacteriorhodopsin. *Biophys. J.* **1999**, *77* (5), 2750−2763.